ACCURACY EVALUATION OF THE POSITIONING OF RPA BY IMAGE

Sidney Andrade de Lima [1], *Daniel Rodrigues Roos* [2], *Gabriel Dietzsch* [3], *Élcio Hideiti Shiguemori* [4] e *Hermann Johann Heinrich Kux* [5]

[1] Institute of Advanced Studies (IEAv), São José dos Campos, SP Mailbox 6044 - 12.228-970 Brazil e e-mail: sidneysal@ieav.cta.br; [2] Institute of Advanced Studies (IEAv), São José dos Campos, SP Mailbox 6044 - 12.228-970 Brazil e e-mail: danielroos@ieav.cta.br; [3] Institute of Advanced Studies (IEAv), São José dos Campos, SP Mailbox 6044 - 12.228-970 Brazil e e-mail: dietzsch@ieav.cta.br; [4] Institute of Advanced Studies (IEAv), São José dos Campos, SP Mailbox 6044 - 12.228-970 Brazil e e-mail: elcio@ieav.cta.br; e [5] National Institute of Space Research (INPE), São José dos Campos, SP Mailbox 515 - 12.227-010 Brazil e e-mail: hermann@dsr.inpe.br

ABSTRACT

The objective of this work is to evaluate the accuracy of the positioning calculation and the guidance of Remotely Piloted Aircraft (RPA) using concepts of photogrammetry from images generated by onboard cameras, aiming at autonomous air navigation. The technique of image navigation uses orthomosaic and Digital Surface Models (DSM) as a reference and images obtained by the onboard camera during flight. When corresponding points are found between these images and the orthomosaic it is possible to calculate the position and attitudes of the perspective center of the camera. With the applied methodology it was possible to verify average errors in the order of 0.5 meters in the positioning and 0.5º in the angle of attitudes of the camera. So the navigation through the image can reach values equal to or higher than the GNSS receivers without differential correction. Therefore, navigating through the image is a good alternative to enable autonomous navigation.

Key words — Autonomy, Navigation, Security, Photogrammetry, Remote Sensing, Spatial Resection and RPA.

1. INTRODUCTION

Currently the use of RPA has increased considerably and became indispensable for several applications where human intervention is dull, dirty and dangerous. For example monitoring of the coast [1], search and rescue operation [2], border surveillance [3], precision agriculture [4], forest control [5], forest fires [6], topography [7], photogrammetry [8] [9] [10], among others.

An application that deserves to be highlighted has been the navigation of RPA, by automatic image processing, that is, determination of its position exclusively from features in images generated by an onboard sensor [11].

For autonomous RPA arrive in a desired location, it must first be known in which position it is. Thus, the information aircraft positioning is importance for navigation, because without it is impossible to navigate autonomously [12].

To solve these problems, one approach is the use of georeferenced images of orbital or airborne sensors of the region of interest and compares them with images obtained at the time of flight. By finding points in common in the two images, the position of the RPA can be determined autonomously [13].

For the navigation of a RPA 3D coordinates and attitudes are required, this information is usually obtained through GNSS and INS. The inertial systems are autonomous and determine their position in space through accelerometers and gyroscopes. However, over time the position and attitude calculation using only the INS becomes inaccurate, because the INS accumulates errors [14].

In addition to the dependence of GNSS there is still concern about the possibility of electronic attacks on the GNSS signal, known as jamming or spoofing interference. These attacks can cut off the GNSS signal or decrease accuracy, causing the RPA to lose its location information or even simulate the GNSS signal and report wrong coordinate positions, and can even take control of the RPA, for more information [15].

One of the approaches for autonomous navigation is the use of automatic terrain recognition techniques in images obtained by onboard sensors [16]. An automatic recognition with orthomosaic and DSM can be employed [11].

In this case for the determination of the three-dimensional coordinates and the angles of attitude of the RPA, it is necessary to consider estimation errors [17] [18]. Through the equations of collinearity and adjustment by the method of least squares [19], it is possible to calculate the coordinates and the attitude of the RPA and their respective accuracy, indispensable to determine when the coordinates obtained by the images will be used to correct the INS.

The primary objective of this article is analyze the accuracies of the coordinate of perspective center and attitude angles of an onboard camera on the RPA. For such, the difference between this calculate coordinate and a reference coordinate coming from the Bundle Block Adjustment (BBA) used to construct the orthomosaic and DSM will be analyzed.

2. MATERIAL AND METHOD

2.1 Collinearity Equations

Projective transformation is a three dimensional transformation. This geometric transformation takes a

system from 3D system (Object Space) to 2D system (Image Space) and vice-versa. The mathematical model that translates this transformation is called the collinearity equation [18]. The collinearity equations are based on the concept that the object space, the perspective center (objective of the camera) and the image space are interconnected by a line.

The 3 rotations between a coordinate system in the Image Space and the Object Space are defined by the parameters Omega (ω), Phi (ϕ) e Kappa (k) presented in Equation 01; being respectively the rotations around the X, Y and Z axes [20].

$$M = \begin{bmatrix} \cos\varphi\cos\kappa & \cos\omega\,sen\,\kappa + sen\,\omega\,sen\,\varphi\cos\kappa & sen\,\omega\,sen\,\kappa - \cos\omega\,sen\,\varphi\cos\kappa \\ -\cos\varphi\,sen\,\kappa & \cos\omega\cos\kappa - sen\,\omega\,sen\,\varphi\,sen\,\kappa & sen\,\omega\cos\kappa + \cos\omega\,sen\,\varphi\,sen\,\kappa \\ sen\,\varphi & -sen\,\omega\cos\varphi & \cos\omega\cos\varphi \end{bmatrix} \quad (1)$$

In Equation 02 and 03 are visualized four parameters, namely: a scale factor (f), and 3 translations (X-Xo), (Y-Yo) e (Z-Zo) between systems. It can be said that this transformation is of the isogonal type, since it has a single scale for the 3 axes of the two systems. In these equations we assemble the Collinearity Equations that connect the Object Space and Image Space, which are non-linear equations [20].

$$x' = (x - x_0) = -f.\frac{a_{11}(X-X_0)+a_{12}(Y-Y_0)+a_{13}(Z-Z_0)}{a_{31}(X-X_0)+a_{32}(Y-Y_0)+a_{33}(Z-Z_0)} \quad (2)$$

$$y' = (y - y_0) = -f.\frac{a_{21}(X-X_0)+a_{22}(Y-Y_0)+a_{23}(Z-Z_0)}{a_{31}(X-X_0)+a_{32}(Y-Y_0)+a_{33}(Z-Z_0)} \quad (3)$$

Where:

- $(x',\ y')$ - coordinates in the fiducial system considering the displacement of the principal point;
- $(x,\ y)$ - coordinates in the fiducial system;
- (x_0, y_0) - coordinates of the principal point in fiducial system;
- (X, Y, Z) - coordinates of the geodetics system;
- (X_0, Y_0, Z_0) - coordinates of the perspective center in geodetics system;
- f - Scale between fiducial and geodetics system; e
- a_{ij} - Parameters by rotation matrix.

2.2 Geometric Distortions in Photographic Images

A raw image contains geometric distortions due to the influence of several intrinsic and extrinsic factors on the sensor. Thus, to obtain reliable metric information from images it is recommended that the sensor be calibrated. The main task in the photogrammetric process is to establish a strict geometric relation between the image and the object, to extract information from object only through the image [18]. The symmetrical radial distortions can be modeled by the even-numbered polynomial equations in the x and y components of the fiducial mark coordinate system. Usually only the coefficients K_1, K_2, and K_3 are used [17].

$$R = \sqrt{x^2 + y^2} \quad (4)$$

$$\delta rx_n = K_1.R^2 + K_2.R^4 + K_3.R^6 + \cdots + K_n.R^{2n} \quad (5)$$

$$\delta ry_n = K_1.R^2 + K_2.R^4 + K_3.R^6 + \cdots + K_n.R^{2n} \quad (6)$$

The tangential distortion comes from the manufacturer's inability to perfectly align the optical axes of the lens that compose an objective, resulting in the displacement of the image pixel. These distortions can be modeled using equations in the x and y components of the fiducial mark coordinate system, usually using only the coefficients p_1 and p_2, as shown in Equations 8 and 9 [18].

$$\delta tx = p_1.(R^2 + 2.x^2) + 2.p_2.x.y \quad (7)$$

$$\delta ty = p_2.(R^2 + 2.y^2) + 2.p_1.x.y \quad (8)$$

In order to obtain a mathematical model that best represents the transformation between the object space and Image space, it is necessary add to the collinearity equations presented in Equations 2 and 3 the respective radial distortions (δrx, δry) and tangents (δtx, δty) in each component, presented in Equations 5, 6, 7 and 8. Besides the distortions, the coordinates of the principal point (x_0, y_0) must also be considered and the scale is represented by the focal length of the camera (f), as shown in Equations 9 and 10.

$$x = x_0 + \delta rx + \delta tx - f.\frac{a_{11}(X-X_0)+a_{12}(Y-Y_0)+a_{13}(Z-Z_0)}{a_{31}(X-X_0)+a_{32}(Y-Y_0)+a_{33}(Z-Z_0)} \quad (9)$$

$$y = y_0 + \delta ry + \delta ty - f.\frac{a_{21}(X-X_0)+a_{22}(Y-Y_0)+a_{23}(Z-Z_0)}{a_{31}(X-X_0)+a_{32}(Y-Y_0)+a_{33}(Z-Z_0)} \quad (10)$$

2.3 Solving Systems of Nonlinear Equations

The resolution of the systems of nonlinear equations is used to calculate the transformation parameters of the collinearity equations, knowing only coordinate of homologous points in the object and image space [17].

For the calculation of the coordinates and attitudes of the perspective center of the camera, at least 3 points are necessary, when the number of equations is greater than the number of unknowns, which in this case is greater than 4 points; we have a possible and indeterminate equations system. To solve this type of equations system and estimated the error, the Least Squares Method (LSM) is used. It can be solved by the matrix method, according to the equations 11, 12 and 13 [19].

$$\Delta X = (J^T.P.J)^{-1}.J^T.P.(L - L_0) \quad (11)$$

$$\bar{X} = X_0 + \Delta X \quad (12)$$

$$\Sigma\bar{X} = |\bar{\sigma}|.(J^T.P.J)^{-1} \quad (13)$$

2.4 Surf and RANSAC

The automatic point identification tests were performed using the Matlab Program and the Speeded Up Robust Features (SURF) [21] and RAndom SAmple Consensus (RANSAC) [22] algorithms. In these cases the identification of the homologous points is performed automatically, that is, without the human interference in the selection of these points [23].

The SURF algorithm performs the description of the characteristics in two images and then makes a correspondence between the characteristic points with the greatest similarity between them. However, these correspondences can cause erroneous matches between the homologous points of the image and orthomosaic. This can occur if one point in the image is more similar to the characteristics of a different point in the orthomosaic.

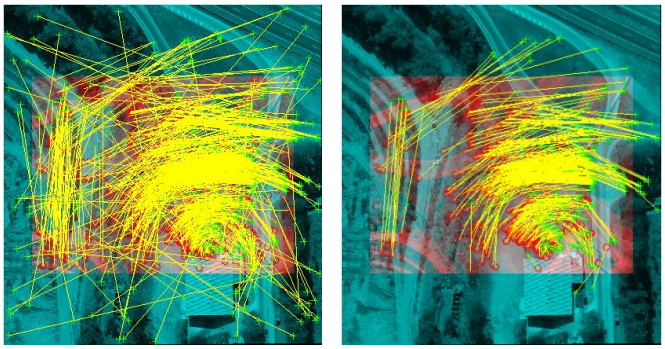

(a) (b)

Figure 1. a) Corresponding points with SURF only and b) Corresponding points with SURF and RANSAC.

Figure 1a shows that in the identification of corresponding points using only the SURF there are some random points in the set of matched point. These points are erroneous identifications, being denominated outliers.

The RANSAC algorithm is used to identify and remove these outliers. Figure 1b shows the set of matched points without the outliers. Although the RANSAC algorithm removes the vast majority of the random points, some outliers can still remain in the set of selected points, being this a factor that can insert errors in the determination of the position and attitude of the camera.

3. RESULTS

Tests were performed using the SURF associated with RANSAC, to remove the outliers. As a consequence, from 39 photographs, only in 6 photographs it was not possible to calculate the spatial resection, since these photographs were oblique. In this case the SURF was not able to identify any of the corresponding points correctly. Two examples of that procedure are depicted in Figures 1a and 1b.

To identify all points correctly a random selection of corresponding points was used. Since even after the removal of outliers by the RANSAC some homologous points may still be erroneously identified, even if the errors are visually small.

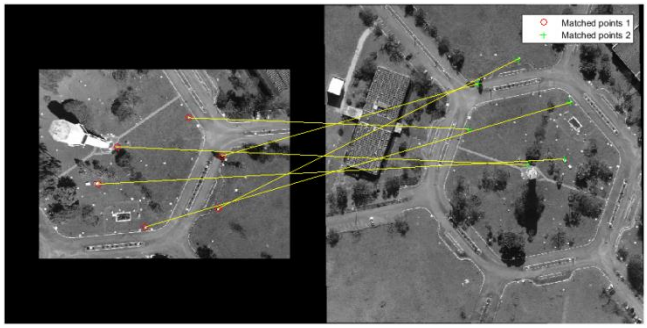

Figure 2. Automatic identification of corresponding points through SURF / RANSAC.

Figure 3 shows the box diagram of the results of the identification of homologous points using the SURF and RANSAC, in red box, algorithms associated to a random search by groups of points, which resulted in a low variance in the determination of the position and attitude of the camera in space. The cyan box represents the positioning errors when the correspondence of points was performed manually.

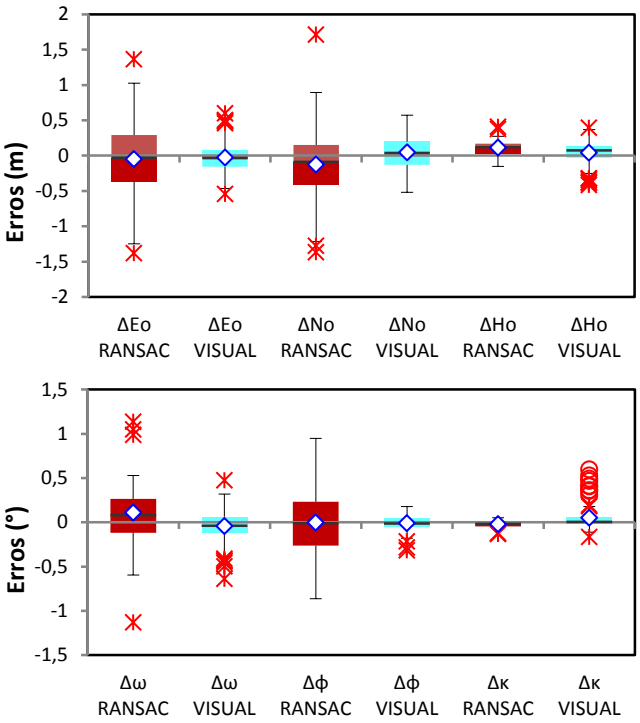

Figure 3. Comparison of error distribution using SURF / RANSAC (Red box) and manually identification (Cyan box).

4. DISCUSSION

In the automatic identification, if there are still outliers among the six points chosen, it is possible to identify them by increasing the spatial resection variance. Thus, an

acceptance value for the variance can be set in order to accept the group of points. If the calculated variance is above the defined value the algorithm performs a new search for another group of points until it finds a group with acceptable variance.

Comparing these results with the results of the manual identification it is verified that on average the positional variances and attitudes, when using the SURF and RANSAC algorithms, are larger than the variances of the manually identified points.

Possibly the largest variances occurred due to errors of identification of homologous points made by SURF and that were small to be identified as outliers by RANSAC. For this reason, they were not removed, resulting in an increase in mean variance. Another factor that possibly influenced the increase of the variance was the grouping of the homologous points in some cases.

5. CONCLUSIONS

From the exposed in Figure 3 it was verified that there was a worsening in the accuracy between SURF/RANSAC method and the manual point's selection. However, when compared to GNSS/INS provided by the Phantom 4 RPA there was a large increase in the accuracy of the data.

The maximum errors ranged from -1.2 to +1.0 meters for Planimetric; -0.2 to +0.3 meters for altimetry and -1.0º to + 1.0º for the attitude angles. Considering the error distribution, of Figure 3 it can be seen that for the positioning of the perspective center the interquartile range did not exceed 0.5m and for the attitude angles the interquartile range did not exceed 0.5º. Such accuracy is better than that provided by the GNSS/INS that does not have differential correction, usually used for real time navigation in most of the RPA.

6. REFERENCES

[1] J. A. Gonçalves and R. Henriques, "RPA photogrammetry for topographic monitoring of coastal areas," ISPRS J. Photogramm. Remote Sens., vol. 104, pp. 101–111, 2015.

[2] J. Roberts, D. Frousheger, B. Williams, D. Campbell, and R. Walker, "How the outback challenge was won," IEEE Robot. Autom. Mag., vol. 23, no. 4, pp. 54–62, 2016.

[3] R. O. ANDRADE, "O voo do falcão." FAPESP, São Paulo, p. v.211, 64-69, 2013.

[4] P. J. Zarco-Tejada, R. Diaz-Varela, V. Angileri, and P. Loudjani, "Tree height quantification using very high resolution imagery acquired from an unmanned aerial vehicle (RPA) and automatic 3D photo-reconstruction methods," Eur. J. Agron., vol. 55, pp. 89–99, 2014.

[5] J. P. Dash, M. S. Watt, G. D. Pearse, M. Heaphy, and H. S. Dungey, "Assessing very high resolution RPA imagery for monitoring forest health during a simulated disease outbreak," ISPRS J. Photogramm. Remote Sens., vol. 131, pp. 1–14, 2017.

[6] H. Sun, G. Song, Z. Wei, Y. Zhang, and S. Liu, "Bilateral teleoperation of an unmanned aerial vehicle for forest fire detection," 2017 IEEE Int. Conf. Inf. Autom. ICIA 2017, no. July, pp. 586–591, 2017.

[7] M. R. James, S. Robson, S. D'Oleire-Oltmanns, and U. Niethammer, "Optimising RPA topographic surveys processed with structure-from-motion: Ground control quality, quantity and bundle adjustment," Geomorphology, vol. 280, pp. 51–66, 2017.

[8] F. C. Nogueira and L. Roberto, "Accuracy analysis of orthomosaic and DSM produced from sensor aboard RPA," XVIII Simpósio Bras. Sensoriamento Remoto -SBSR, vol. d, no. 2011, pp. 4880–4887, 2017.

[9] F. Agüera-Vega, F. Carvajal-Ramírez, and P. Martínez-Carricondo, "Assessment of photogrammetric mapping accuracy based on variation ground control points number using unmanned aerial vehicle," Meas. J. Int. Meas. Confed., vol. 98, pp. 221–227, 2017.

[10] F. Agüera-Vega, F. Carvajal-Ramírez, and P. Martínez-Carricondo, "Accuracy of Digital Surface Models and Orthomosaics Derived from Unmanned Aerial Vehicle Photogrammetry," J. Surv., vol. 143, no. 2, pp. 1–10, 2016.

[11] J. R. G. Braga, H. F. de Campos Velho, G. Conte, P. Doherty, and E. H. Shiguemori, "An Image Matching System for Autonomous RPA Navigation Based on Neural Network," International Conference on Control, Automation, Robotics & Vision (ICARCV), Phuket, Thailand, p. 6, 2016.

[12] C. F. Lo et al., "The direct georeferencing application and performance analysis of RPA helicopter in GCP-free area," ISPRS - Int. Arch. Photogramm. Remote Sens. Spat. Inf. Sci., vol. XL-1/W4, no. 1W4, pp. 151–157, Aug. 2015.

[13] S. A. Lima, L. Roberto, E. H. Shiguemori, H. J. H. Kux, and J. L. N. e S. Brito, "Determinação da posição e atitudes de VANT por fotogrametria," XVIII Simpósio Bras. Sensoriamento Remoto - SBSR, no. 2008, pp. 5392–5399, 2017.

[14] G. Conte and P. Doherty, "a Visual Navigation System for RPA Based on Geo-Referenced Imagery," ISPRS - Int. Arch. Photogramm. Remote Sens. Spat. Inf. Sci., vol. XXXVIII-1/, no. September, pp. 1–6, 2011.

[15] L. de A. Faria, C. A. de M. Silvestre, and M. A. F. Correia, "GPS-dependent systems: Vulnerabilities to electromagnetic attacks," J. Aerosp. Technol. Manag., vol. 8, no. 4, pp. 423–430, 2016.

[16] P. F. F. Silva Filho, "Automatic Landmark Recognition in Aerial Images for the Autonomous Navigation System of Unmanned Aerial Vehicles," Instituto Tecnológico de Aeronautica - ITA, São José dos Campos, 2016.

[17] P. R. Wolf, B. A. Dewitt, and B. E. Wilkinson, Elements of Photogrammetry with Applications in GIS. New York: Mc Graw Hill Education, 2014.

[18] J. C. McGlone and G. Y. G. Lee, Manual of Photogrammetry, Sixth. Bethesda, 2013.

[19] C. D. Ghilani, Adjustament Computations: Spatial Data Analysis. New Jersey: Wily, 2017.

[20] E. M. Mikhail, J. S. Bethel, and J. C. McGlone, Introduction to Modern Photogrammetry. Hobeken: Wiley, 2001.

[21] H. Bay and A. Ess, "Speeded-Up Robust Features (SURF)," vol. 110, pp. 346–359, 2008.

[22] M. A. Fischler and R. C. Bolles, "Random Sample Consensus : A Paradigm for Model Fitting with Applications to Image Analysis and Automated Cartography," Commun. ACM, vol. v. 24, , pp. 381–395, 1981.

[23] D. R. Roos, "Aprendizado de Máquina Aplicado a Odometria Visual para estimação de posição de Veículos Aéreos Não Tripulados," Universidade Federal de São Paulo, 2018.